Research Square

Preprints are preliminary reports that have not undergone peer review.
They should not be considered conclusive, used to inform clinical practice,
or referenced by the media as validated information.

Spectral Analysis of Dynamic Long-Axial-Field-of-View PET: A Flexible Framework for Whole-Body Multi-Organ Kinetic Quantification

Fengyun Gu

fengyungu@126.com

North China Electric Power University

Qi Wu

University College Cork

Shen Ni

North China Electric Power University

Ruiqing Ni

University of Bern

Axel Rominger

University of Bern

Kuangyu Shi

University of Bern

Research Article

Keywords: Dynamic LAFOV PET, Multi-Organ Kinetics, Spectral Analysis, Tracer Delay, Whole-Body Parametric Imaging

Posted Date: May 12th, 2026

DOI: https://doi.org/10.21203/rs.3.rs-9658551/v1

License: This work is licensed under a Creative Commons Attribution 4.0 International License.
Read Full License

Additional Declarations: The authors declare no competing interests.

Spectral Analysis of Dynamic Long-Axial-Field-of-View PET: A Flexible Framework for Whole-Body Multi-Organ Kinetic Quantification

Fengyun Gu[1,2], Qi Wu[3,4], Shen Ni[1], Ruiqing Ni[2], Axel Rominger[2], Kuangyu Shi[2]

[1] School of Mathematics and Physics, North China Electric Power University, Beijing, China

[2] Department of Nuclear Medicine, Inselspital, Bern University Hospital, University of Bern, Bern, Switzerland

[3] School of Mathematical Sciences, University College Cork, Cork, Ireland

[4] Insight Centre for Data Analytics, Cork, Ireland

Corresponding author: Fengyun Gu, Email: fengyungu@126.com

Abstract

Purpose: Although long-axial-field-of-view (LAFOV) PET systems are increasingly installed worldwide, quantitative analysis of dynamic LAFOV PET is still mainly based on compartmental models or graphical methods, which may be inadequate for whole-body imaging due to the complexity and heterogeneity of multi-organ tracer kinetics. The purpose of this study is to investigate the feasibility of spectral analysis and explore its adaptation for whole-body kinetic quantification at both volume of interest (VOI) and voxel levels.

Methods: Spectral analysis (SA) models the impulse response function as a sum of exponential terms, enabling flexible representation of diverse tracer kinetics. We extend SA to a whole-body quantification framework by incorporating fractional blood volume and tracer arrival time delays. To improve robustness at the voxel level, spectral analysis with iterative filtering (SAIF) is employed for parametric image generation within the same framework. The methodology is evaluated in 24 cancer patients who underwent dynamic ^{18}F-FDG PET/CT scans on a LAFOV system. A comprehensive comparison is performed among standard SA and SAIF, as well as their corresponding implementations within the proposed whole-body framework at both VOI and voxel levels.

Results: Spectral analysis with the proposed whole-body framework (SA*) achieves the best fits to VOI time activity curves across most organs, as reflected by consistently lower Akaike information criterion (AIC) values, particularly in tissues with complex kinetics such as the liver and kidney. Estimates of ^{18}F-FDG flux are generally consistent across methods. However, substantial differences are observed in vascular blood volume, volume of distribution, and flow-related parameters. At the voxel level, spectral analysis with iterative filtering within the proposed framework (SAIF*) provides the most stable and spatially consistent parametric images with substantial noise reduction compared with standard implementations.

Conclusion: This work presents the first systematic evaluation of spectral analysis in dynamic LAFOV PET. The proposed framework enables flexible quantification of whole-body multi-organ kinetics and enhances parametric imaging, with potential to support clinical decision-making.

Keywords: *Dynamic LAFOV PET, Multi-Organ Kinetics, Spectral Analysis, Tracer Delay, Whole-Body Parametric Imaging*

1 Introduction

The advent of long–axial-field-of-view (LAFOV) PET systems has fundamentally transformed molecular imaging by enabling dynamic acquisition of tracer kinetics across the entire body [1–4]. This capability provides a unique opportunity to simultaneously investigate physiologic processes across multiple organs, moving beyond traditional single-organ imaging toward system-level characterization of human biology. Recent studies have demonstrated the potential of dynamic total-body PET for quantifying organ-specific perfusion [5], metabolism [6], and inter-organ interactions [7], highlighting its value for studying complex diseases involving multiple organ systems.

Despite these advances, quantitative analysis of dynamic LAFOV PET data remains challenging. A key limitation arises from the pronounced heterogeneity of tracer kinetics across different organs and tissues. Conventional compartmental modeling approaches, which require predefined model structures, are often inadequate in this setting because the optimal model may vary across organs, tissues, and even individual voxels. Recent work has emphasized the need for voxelwise model selection and delay

correction strategies [5,8–10], further underscoring the complexity and lack of scalability of traditional modeling frameworks for whole-body applications. Efforts have also been made to relax the exponential assumptions underlying these models, for example through adapted exponential formulations such as the adiabatic approximation to tissue homogeneity (AATH) model [11], as well as fully non-parametric approaches that do not impose a predefined functional form [12–14]. Alternative approaches such as graphical analysis and simplified parametric imaging methods have been proposed to improve computational efficiency and clinical feasibility [15–20]. However, these methods rely on restrictive assumptions regarding tracer kinetics and typically provide only limited macroparametric information, without fully characterizing the underlying dynamic processes. For the comprehensive overview of recent methodological advances, readers are referred to our recent review papers [21, 22].

Spectral analysis provides a data-driven approach for dynamic PET quantification [23]. By representing the tissue impulse response function as a weighted sum of exponential components, it avoids the need for specifying a fixed compartmental model and naturally accommodates a broad range of kinetic behaviors [24]. To enhance its robustness at voxel level, several methodological improvements have been proposed. For example, spectral analysis with iterative filtering (SAIF) [25] and rank-shaping spectral analysis [26] have been developed to effectively reduce noise and improve the stability of parametric image estimation. These developments, together with numerous applications in brain and regional studies, have demonstrated the flexibility of spectral analysis in capturing complex tracer dynamics and tissue heterogeneity [27–33]. However, to date, its application in dynamic LAFOV PET remains largely underexplored. Apart from a recent conference report by Boellaard et al. [34], the formal evaluation of SA in LAFOV PET imaging has yet to appear in the literature. This limited adoption is likely due to practical challenges in implementation. Currently, there are no available open-source tools dedicated to SA [22]. Previously developed software such as SAKE is no longer actively maintained [35], while commercial platforms such as PMOD provide only partial support and lack specific optimization for dynamic LAFOV PET studies.

In this study, we propose a generalized spectral analysis framework for dynamic LAFOV PET that incorporates fractional blood volume and tracer arrival time delay, and extends to voxel-level parametric imaging using iterative filtering strategies. The method is evaluated in a cohort of pa-

tients undergoing dynamic ^{18}F-FDG PET on a LAFOV system, with a comprehensive comparison of standard spectral analysis, spectral analysis with iterative filtering, and their corresponding implementations within the proposed whole-body framework at both volume of interest (VOI) and voxel levels. To the best of our knowledge, this study provides the first formal evaluation of spectral analysis in dynamic LAFOV PET and establishes a flexible approach for whole-body multi-organ kinetic quantification.

2 Materials and Methods

2.1 Patient Scans

Twenty-four patients with various cancer types underwent dynamic ^{18}F-FDG PET/CT imaging on a Biograph Vision Quadra scanner at Bern University Hospital. List-mode acquisition started 15 s before intravenous bolus injection of ^{18}F-FDG into either the left or the right arm. Emission data were acquired for 65 min and reconstructed into 62 contiguous time frames with the following frame durations: 2×10 s, 30×2 s, 4×10 s, 8×30 s, 4×60 s, 5×120 s, and 9×300 s. PET images were reconstructed with a voxel size of $1.65\times1.65\times1.65$ mm^3. Low-dose CT images acquired as part of the PET/CT examination were reconstructed with a voxel size of $1.52\times1.52\times1.65$ mm^3. Further details of the imaging protocol have been reported previously [18]. Representative dynamic PET images are shown in Figure 1. Several volumes of interest (VOIs) are delineated for major normal tissues, including gray matter (GM), white matter (WM), lung, liver, spleen, kidney, bladder, and bone, as well as tumor lesions when present, following the same procedure as in our previous work [14]. Corresponding time activity curves (TACs) are extracted from the dynamic PET images.

2.2 Whole-Body PET Quantification Framework

Dynamic PET data are commonly interpreted under the indicator-dilution theory [36], in which the measured tissue time activity curve (C_T) is expressed as the convolution of the arterial input function

(C_p) with the tissue impulse response function (R):

$$C_T(t) = \int_0^t R(t-s)C_p(s)\,ds \equiv R(t) \otimes C_p(t). \tag{1}$$

The arterial input function is ideally obtained through arterial blood sampling, although this approach is rarely feasible in LAFOV PET studies [37–39]. Instead, an image-derived input function (IDIF) is typically extracted from a large arterial structure such as the descending aorta (DA). Because this measurement location is often spatially separated from the tissue of interest, a temporal delay is introduced between the measured input and the actual tracer arrival in tissue. Delay effects are commonly neglected in conventional PET studies, where limited spatial coverage and relatively coarse temporal sampling reduce their impact. With dynamic LAFOV PET, however, tracer arrival times can vary substantially across organs due to differences in vascular transport. These tracer arrival time delays, which may reach tens of seconds or longer, have been shown to significantly affect kinetic parameter estimation if not accounted for [8, 9, 40].

The measured PET signal also contains a vascular component. This contribution is often negligible in brain imaging but becomes increasingly important in whole-body studies, where the fractional blood volume varies across organs and may represent a substantial portion of the measured activity, particularly in highly vascularized tissues or near large vessels.

To account for both temporal delay and vascular contribution, the standard convolution model is adapted by incorporating a delay term (Δ) and a fractional blood volume term (V_B):

$$C_T(t) = V_B\, C_p(t-\Delta) + (1-V_B) \int_0^t R(t-s)C_p(s-\Delta)\,ds. \tag{2}$$

This formulation provides a more physiologically consistent description of tracer kinetics in dynamic LAFOV PET, capturing both inter-organ variability in tracer arrival and the vascular contribution to the measured signal.

2.3 Spectral Analysis

Spectral analysis (SA) represents the tissue impulse response function as a non-negative weighted sum of exponential basis functions [23]:

$$R(t) = \sum_{j=0}^{J} \alpha_j e^{-\beta_j t}, \qquad \alpha_j \geq 0,\ \beta_j \geq 0,\ \beta_0 = 0. \tag{3}$$

Here, $J+1$ denotes the maximum number of spectral basis functions. The decay constants β_j are pre-defined to cover a physiologically relevant range of kinetic components, whereas the coefficients α_j are estimated from the dynamic PET data and constitute the kinetic spectrum. In this study, 100 basis functions are used, with β_j values distributed over the range 0.03–30 min^{-1}, including $\beta_0 = 0$ to represent the irreversible trapping component.

Substituting Eq. (3) into the whole-body quantification model in Eq. (2) gives

$$C_T(t) = V_B C_p(t-\Delta) + (1-V_B) \sum_{j=0}^{J} \alpha_j \left[e^{-\beta_j t} \otimes C_p(t-\Delta) \right]. \tag{4}$$

The unknown parameter vector is therefore: $\theta = [\Delta, V_B, \alpha_0, \alpha_1, \ldots, \alpha_J]$. Because the model is linear in V_B and α_j for a fixed delay Δ, parameter estimation is performed by a grid-search strategy over Δ combined with non-negative least squares estimation of the remaining parameters. Specifically, Δ is searched from -60 s to 60 s with a step size of 0.5 s. For each candidate delay, the delayed input function is generated, the corresponding spectral basis functions are constructed, and V_B and α_j are estimated under non-negativity constraints using non-negative least squares. The optimal delay is selected as the value yielding the minimum residual sum of squares. This procedure preserves the linear estimation structure of spectral analysis while allowing correction for tracer arrival delay and vascular contribution.

This formulation provides a flexible representation of tracer kinetics without requiring a pre-specified compartmental structure. The resulting spectrum can be used to infer model structure such as the number of components, reversibility, and irreversible uptake [24, 41]. The associated kinetic

parameters such as flow (K_1), flux (K_i) and total volume of distribution (V_T) are computed as

$$K_1 = \sum_{j=0}^{J} \alpha_j, \qquad K_i = \alpha_0, \qquad V_T = \sum_{j=1}^{J} \frac{\alpha_j}{\beta_j}. \tag{5}$$

2.4 Spectral Analysis with Iterative Filter

Spectral analysis with iterative filter introduces a bandpass filter in the spectral domain to separate physiologically meaningful equilibrating components from components associated with tracer trapping, vascular activity, or noise [25]. Following an initial SA estimation, the spectral components are filtered according to their decay constants β_j. Components within a predefined bandpass $[\beta_L, \beta_U]$ are retained as equilibrating components, whereas components outside this interval are removed. In this study, the bandpass is defined as $\beta_L = 0.05$ min^{-1} and $\beta_U = 3$ min^{-1}.

Because removal of spectral components alters the estimates of the remaining trapping and vascular contributions, the estimation and filtering steps are repeated iteratively. At each iteration, the filtered spectrum is used to reconstruct the tissue time activity curve, and the spectral coefficients are re-estimated under non-negativity constraints using the same framework as standard spectral analysis. The delay term and fractional blood volume are incorporated using the same grid-search and estimation procedure described above, resulting in the adapted SAIF model. Kinetic parameters are then computed from the final filtered spectrum using Eq. (5).

2.5 Statistical Analysis

Model performance is evaluated using the Akaike information criterion (AIC), computed from VOI-based TAC fitting for all four methods. Lower AIC values indicate a better trade-off between model fit and complexity. Pearson correlation coefficients are calculated to assess the agreement of kinetic parameters between spectral analysis and the adapted spectral analysis across the 24 patients.

For each VOI, kinetic parameters and the number of spectral components are summarized across patients using the mean and standard deviation (SD), providing an overall characterization of inter-patient variability. Differences in VOI-based kinetic parameters between methods are assessed using the Wilcoxon signed-rank test. This nonparametric test is used to evaluate paired differences without

assuming normality of the data. A two-sided $p \leq 0.05$ is considered statistically significant.

3 Results

3.1 Performance of Spectral Analysis Methods to Regional Time Activity Curves

Representative TAC fits across nine VOIs are presented in Figure 2 and the corresponding kinetic spectrums for each VOI are provided in Supplemental Figure S1. For most organs, all methods provide generally reasonable agreement with the measured data over the full dynamic acquisition. However, clear differences emerge in the early phase (0–3 min), where the delay-adapted approaches (SA* and SAIF*) more accurately capture the early kinetics across multiple organs. This improvement is particularly evident in tissues with more complex kinetics such as the lung, spleen, and kidney, where standard implementations (SA and SAIF) exhibit noticeable temporal mismatches.

Certain VOIs are not well described by spectral analysis–based approaches. In particular, bladder TACs show systematic deviations between measured data and model fits across all methods, reflecting the inherent limitations of the exponential impulse response function in strongly accumulating kinetics. In addition, even with delay-adapted methods, the early phase of the liver TAC remained poorly fitted.

Quantitative comparison using AIC values further supports these observations. The distribution of AIC values is shown as boxplots in Figure 3, and summary statistics (mean and standard deviation) for each VOI across 24 subjects are provided in Supplemental Table S1. SA* and SAIF* achieve lower AIC values than SA and SAIF across all regions, demonstrating improved goodness-of-fit when delay correction is incorporated. Among the four methods evaluated, SA* provides the best overall fit at the VOI level. This is consistent with the fact that SA is primarily designed for VOI-based analysis, whereas SAIF is optimized for noise reduction at the voxel level and may therefore compromise precision. These results highlight the clear advantage of the proposed whole-body adapted spectral analysis approach.

3.2 Regional Kinetic Parameter Estimates from VOI analysis

Regional kinetic parameters and associated delay estimates (where applicable) derived from the four spectral analysis methods across nine volumes of interest in 24 subjects are presented in Table 1. Delay estimates are reported only for SA* and SAIF*, with values varying across VOIs and showing differences in tracer arrival timing between tissues. Notably, although delay values are also obtained for the bladder, these estimates are not considered meaningful given the known limitations of spectral analysis in modeling bladder kinetics.

For K_i and V_T, estimates are generally consistent across all four methods for most VOIs. Slight differences are observed in organs such as the liver and kidney, where the inclusion of delay results in modest changes in these parameters. In contrast, more noticeable differences are observed for flow-related parameters, such as K_1 and V_B. In particular, SAIF tends to yield systematically lower V_B values across most regions, whereas the delay-adapted methods (SA* and SAIF*) produce higher V_B estimates in several organs, including the kidney and spleen. Wilcoxon signed-rank test p-values for VOI kinetic parameters across different methods are provided in Supplemental Table S2.

To further examine the relationships among the kinetic parameters obtained at the VOI level, we compare the estimates derived from SA and SA*. Since SA is originally designed primarily for VOI analysis, this direct comparison provides additional insight into the quantitative effect of incorporating delay correction. As shown in Figure 4, delay adaptation has little effect on the estimates of K_i and V_T, both of which remain highly consistent between SA and SA* ($R = 0.999$ and $R = 0.988$, respectively). But larger differences are observed for K_1 and V_B, with lower correlations between SA and SA* ($R = 0.872$ and $R = 0.689$, respectively), indicating that these flow-related parameters are more strongly affected by delay correction.

Furthermore, the flexibility of spectral analysis for multi-organ kinetic quantification is well demonstrated by its ability to determine the optimal number of spectral components for each VOI directly from the data. As summarized in Table 2, this number varies across regions but remains generally consistent across the four methods for each individual VOI, with only minor differences observed between methods.

3.3 Parametric Imaging

Representative parametric images derived from the four spectral analysis methods are shown in Figure 5. Among the four parameters, K_i shows the highest consistency across methods, with very similar spatial distributions. This is expected since K_i primarily reflects late-time kinetics and is less sensitive to temporal misalignment. In contrast, more pronounced differences are observed for K_1, V_T, and V_B across methods, with greater variability in several organs.

The delay effect is most evident in highly perfused regions, most notably the heart, where SA* and SAIF* produce more localized and physiologically plausible patterns. This highlights the importance of accounting for arrival time differences in whole-body dynamic imaging, where inter-organ delays are non-negligible.

Although conventional SA is primarily designed for VOI-level analysis, its voxel-level performance remains acceptable in the current data. This is likely due to the increased sensitivity of LAFOV PET, which improves count statistics at the voxel level and enables stable estimation of parametric maps even without additional regularization.

Across the four methods, SAIF* provides the best overall voxel-level performance, reducing noise while maintaining consistent kinetic patterns. Compared with SAIF, it also alleviates the loss of quantitative accuracy introduced by smoothing, as observed in specific regions, such as the kidney on V_B maps and the brain on K_1 maps.

3.4 Spatial Distribution of Estimated Time Delays and Number of Components

Voxel-wise tracer arrival delay maps are shown in Figure 6. Clear spatial variations in delay are observed across organs. The lungs show negative delays relative to the arterial input reference, whereas positive delays are observed in other tissues. The estimated delays span approximately ± 60 seconds, with the largest values observed near the body surface. The overall spatial patterns are consistent between SA* and SAIF*, with only minor local differences.

The spatial distribution of the optimal number of spectral components is shown in Figure 7. The estimated number of components varies across organs, indicating heterogeneous kinetic complexity at

the voxel level. Despite this variability, similar spatial patterns are observed across the four methods, with comparable component numbers selected in most regions and only localized differences between methods. These results indicate that delay incorporation and smoothing have limited impact on the estimated number of components.

4 Discussion

This work provides the first systematic evaluation of spectral analysis for dynamic LAFOV PET imaging. A key strength of spectral analysis lies in its flexibility, as it does not require prior assumptions about the model order of the tissue response function. Instead, the spectral profile itself implicitly determines the underlying model structure, making it particularly suitable for capturing the complex and heterogeneous kinetics observed in whole-body imaging. Such a data-driven formulation is conceptually analogous to recent model selection strategies in LAFOV PET, where different compartment models are selected for individual voxels or tissues [9, 10, 43]. However, spectral analysis extends this idea by avoiding explicit model specification altogether, providing a more flexible and unified framework for describing multi-organ kinetics.

Another important aspect in extending spectral analysis to whole-body LAFOV PET is the correction of tracer arrival delays. In current LAFOV PET quantification, delay effects have mainly been investigated within compartmental modeling frameworks [8, 9, 40, 44–46]. Delay in spectral analysis has received relatively limited attention, with previous studies typically considering a single global delay in brain-specific applications [47]. In the whole-body setting, substantial inter-organ differences in tracer arrival time are observed, making a single global delay inadequate. The present results show that accounting for region-specific delays improves the representation of early kinetics and leads to more consistent parameter estimates across organs, particularly for perfusion-related parameters.

The same dataset has previously been analyzed using conventional approaches, including compartmental modeling and Patlak analysis [18]. Within this context, the adapted spectral analysis framework shows improved characterization for most organs, although unsatisfied performance is still observed in regions such as the liver and bladder. This behavior can be linked to the exponential

assumption imposed on the response function, which limits the ability of spectral analysis to represent more complex or non-standard kinetic patterns. Our previous study using non-parametric approach has demonstrated robust performance in modeling such kinetics, given their ability to accommodate both exponential and non-exponential response functions [14], supporting the interpretation that the observed limitations are primarily driven by the underlying model assumption rather than the data itself.

A long-standing challenge in applying spectral analysis for parametric imaging is its sensitivity to voxel-level noise. To address this limitation, several variants have been proposed, including rank-shaping spectral analysis [48] and SAIF. Among these, SAIF is particularly attractive as it preserves the full kinetic profile while incorporating noise suppression, and is therefore adopted in this work. In the context of LAFOV PET, this limitation is partially mitigated due to the substantially improved voxel-level count statistics. As a result, spectral analysis can already produce stable parametric images. Even in this setting, adapted SAIF remains advantageous by further reducing voxel-level noise and yielding smoother and more reliable parametric maps, thereby providing enhanced robustness for voxel-wise quantification.

Reliable uncertainty quantification plays a central role in the clinical use of parametric imaging, as it enables confidence in voxel-wise estimates and supports decision-making. Bootstrap-based approaches have previously been applied to spectral analysis for uncertainty estimation [49]. However, the substantially increased data volume in LAFOV PET introduces significant computational challenges, limiting the practicality of conventional bootstrap methods. Alternative strategies such as image-domain bootstrap approaches [14, 50], provide a feasible pathway for uncertainty assessment in large-scale dynamic datasets. Integrating such strategies with spectral analysis would allow comprehensive uncertainty characterization at the whole-body level, further facilitating its translation to clinical applications.

5 Conclusion

This study provides the first systematic evaluation of spectral analysis for dynamic LAFOV PET imaging. By incorporating fractional blood volume and region-specific tracer delays, the proposed framework enables flexible modeling of heterogeneous whole-body kinetics without explicit model selection. The results demonstrate improved characterization of early kinetics and consistent parameter estimation across organs, with enhanced voxel-level robustness achieved through adapted SAIF. Despite remaining limitations in organs with complex kinetics, such as the liver and bladder, this work establishes spectral analysis as a viable and scalable approach for whole-body parametric imaging in LAFOV PET.

Disclosure

The local Institutional Review Board approved the study (KEK 2019–02193), and written informed consent was obtained from all patients. The study was performed in accordance with the declaration of Helsinki.

Acknowledgements

This work was supported in part by the Fundamental Research Funds for the Central Universities, China (2026MS089) and a grant from Research Ireland under Grant number 12-RC-2289-P2 which is co-funded under the European Regional Development Fund.

References

[1] Badawi Ramsey D, Shi Hongcheng, Hu Pengcheng, et al. First Human Imaging Studies with the EXPLORER Total-Body PET Scanner. *Journal of Nuclear Medicine.* 2019;60:299–303.

[2] Pantel Austin R, Viswanath Varsha, Daube-Witherspoon Margaret E, et al. PennPET Explorer: human imaging on a whole-body imager. *Journal of Nuclear Medicine.* 2020;61:144–151.

[3] Alberts Ian, Hünermund Jan-Niklas, Prenosil George, et al. Clinical performance of long axial field of view PET/CT: a head-to-head intra-individual comparison of the Biograph Vision Quadra with the Biograph Vision PET/CT. *European journal of nuclear medicine and molecular imaging.* 2021;48:2395–2404.

[4] Zhang Haiqiong, Ren Chao, Liu Yu, et al. Performance Characteristics of a New Generation 148-cm Axial Field-of-View uMI Panorama GS PET/CT System with Extended NEMA NU 2-2018 and EARL Standards. *Journal of Nuclear Medicine.* 2024;65:1974–1982.

[5] Knuuti Juhani, Tuisku Jouni, Kärpijoki Henri, et al. Quantitative perfusion imaging with total-body PET. *Journal of Nuclear Medicine.* 2023;64:11S–19S.

[6] Liu Guobing, Xu Hongrong, Hu Pengcheng, et al. Kinetic metrics of 18F-FDG in normal human organs identified by systematic dynamic total-body positron emission tomography. *European Journal of Nuclear Medicine and Molecular Imaging.* 2021;48:2363–2372.

[7] Sun Tao, Wang Zhenguo, Wu Yaping, et al. Identifying the individual metabolic abnormities from a systemic perspective using whole-body PET imaging. *European Journal of Nuclear Medicine and Molecular Imaging.* 2022:1–11.

[8] Feng Tao, Zhao Yizhang, Shi Hongcheng, et al. Total-body quantitative parametric imaging of early kinetics of 18F-FDG. *Journal of Nuclear Medicine.* 2021;62:738–744.

[9] Wang Guobao, Nardo Lorenzo, Jones Terry, et al. Total-Body PET Multiparametric Imaging of Cancer Using a Voxel-wise Strategy of Compartmental Modeling. *Journal of Nuclear Medicine.* 2021.

[10] Åhlström Anna, Lindström Elin, Maaniitty Teemu, et al. Automated Total-Body Perfusion Imaging with 15O-Water PET Using Basis Functions and Organ-Specific Model Selection. *Journal of Nuclear Medicine.* 2025;66:1307–1313.

[11] Chung Kevin J, Chaudhari Abhijit J, Nardo Lorenzo, et al. Quantitative total-body imaging of blood flow with high-temporal-resolution early dynamic 18F-FDG PET kinetic modeling. *Journal of Nuclear Medicine.* 2025;66:973–980.

[12] O'Sullivan Finbarr, Muzi Mark, Mankoff David A, et al. Voxel-level mapping of tracer kinetics in PET studies: a statistical approach emphasizing tissue life tables. *The annals of applied statistics.* 2014;8:1065.

[13] Gu Fengyun, O'Sullivan Finbarr, Muzi Mark, et al. Quantitation of multiple injection dynamic PET scans: an investigation of the benefits of pooling data from separate scans when mapping kinetics. *Physics in Medicine & Biology.* 2021;66:135010.

[14] Wu Qi, Gu Fengyun, O'Suilleabhain Liam D., et al. Mapping 18F-FDG Kinetics Together with Patient-Specific Bootstrap Assessment of Uncertainties: An Illustration with Data from a PET/CT Scanner with a Long Axial Field of View. *Journal of Nuclear Medicine.* 2024;65:971–979.

[15] Patlak Clifford S, Blasberg Ronald G, Fenstermacher Joseph D. Graphical evaluation of blood-to-brain transfer constants from multiple-time uptake data. *Journal of Cerebral Blood Flow & Metabolism.* 1983;3:1–7.

[16] Gu Fengyun, Wu Qi, Wu Jianmao, et al. Feasibility of standard and generalized Patlak Models for dynamic imaging of multiple organs using the uEXPLORER PET scanner. *Journal of Nuclear Medicine.* 2022;63:3185–3185.

[17] Zhang Xuezhu, Xie Zhaoheng, Berg Eric, et al. Total-body dynamic reconstruction and parametric imaging on the uEXPLORER. *Journal of Nuclear Medicine.* 2020;61:285–291.

[18] Sari Hasan, Mingels Clemens, Alberts Ian, et al. First results on kinetic modelling and parametric imaging of dynamic 18F-FDG datasets from a long axial FOV PET scanner in oncological patients. *European journal of nuclear medicine and molecular imaging.* 2022:1–13.

[19] Karakatsanis Nicolas, Angelis Georgios, Bailey Dale, et al. Total-body direct 18F-FDG generalized patlak imaging for superior multi-parametric PET quantification in oncology. *Journal of Nuclear Medicine.* 2025;66(252013).

[20] Li Siqi, Abdelhafez Yasser G, Nardo Lorenzo, et al. Total-body parametric imaging using relative Patlak plot. *Journal of Nuclear Medicine.* 2025;66:654–661.

[21] Gu Fengyun, Wu Qi. Quantitation of dynamic total-body PET imaging: recent developments and future perspectives. *European Journal of Nuclear Medicine and Molecular Imaging.* 2023;50:3538–3557.

[22] Gu Fengyun, Mingels Clemens, Seifert Robert, et al. Parametric imaging of dynamic long-axial-field-of-view PET scans: Technical challenges, statistical insights and clinical applications. *Zeitschrift für Medizinische Physik.* 2026.

[23] Cunningham Vincent J, Jones Terry. Spectral analysis of dynamic PET studies. *Journal of Cerebral Blood Flow & Metabolism.* 1993;13:15–23.

[24] Veronese Mattia, Rizzo Gaia, Bertoldo Alessandra, et al. Spectral analysis of dynamic PET studies: a review of 20 years of method developments and applications. *Computational and mathematical methods in medicine.* 2016;2016.

[25] Veronese Mattia, Bertoldo Alessandra, Bishu Shrinivas, et al. A spectral analysis approach for determination of regional rates of cerebral protein synthesis with the L-[1-11C] leucine PET method. *Journal of Cerebral Blood Flow & Metabolism.* 2010;30:1460–1476.

[26] Turkheimer Federico E, Hinz Rainer, Gunn Roger N, et al. Rank-shaping regularization of exponential spectral analysis for application to functional parametric mapping. *Physics in Medicine & Biology.* 2003;48:3819.

[27] Turkheimer F, Moresco ROSA MARIA, Lucignani G, et al. The use of spectral analysis to determine regional cerebral glucose utilization with positron emission tomography and [18F] fluo-

rodeoxyglucose: theory, implementation, and optimization procedures. *Journal of Cerebral Blood Flow & Metabolism.* 1994;14:406–422.

[28] Bertoldo Alessandra, Vicini Paolo, Sambuceti Gianmario, et al. Evaluation of compartmental and spectral analysis models of [/sup 18/F] FDG kinetics for heart and brain studies with PET. *IEEE transactions on biomedical engineering.* 1998;45:1429–1448.

[29] Tomasi Giampaolo, Kenny Laura, Mauri Francesco, et al. Quantification of receptor-ligand binding with [18F] fluciclatide in metastatic breast cancer patients. *European journal of nuclear medicine and molecular imaging.* 2011;38:2186–2197.

[30] Rizzo Gaia, Veronese Mattia, Zanotti-Fregonara Paolo, et al. Voxelwise quantification of [11C](R)-rolipram PET data: a comparison between model-based and data-driven methods. *Journal of Cerebral Blood Flow & Metabolism.* 2013;33:1032–1040.

[31] Grecchi Elisabetta, Veronese Mattia, Moresco Rosa Maria, et al. Quantification of dynamic [18F] FDG PET studies in acute lung injury. *Molecular imaging and biology.* 2016;18:143–152.

[32] Fan Zhen, Dani Melanie, Femminella Grazia D, et al. Parametric mapping using spectral analysis for 11C-PBR28 PET reveals neuroinflammation in mild cognitive impairment subjects. *European Journal of Nuclear Medicine and Molecular Imaging.* 2018;45:1432–1441.

[33] Veronese Mattia, Tuosto Marcello, Marques Tiago Reis, et al. Parametric mapping for TSPO PET imaging with spectral analysis impulsive response function. *Molecular Imaging and Biology.* 2021;23:560–571.

[34] Boellaard Ronald, Smith Charlotte, Zwezerijnen Gerben, et al. Spectral analysis of dynamic large axial field of view PET/CT studies. in *Journal of Nuclear Medicine*;65:241174 2024.

[35] Veronese Mattia, Rizzo Gaia, Turkheimer Federico E., et al. SAKE: A new quantification tool for positron emission tomography studies. *Computer Methods and Programs in Biomedicine.* 2013;111:199–213.

[36] Meier Paul, Zierler Kenneth L. On the theory of the indicator-dilution method for measurement of blood flow and volume. *Journal of applied physiology.* 1954;6:731–744.

[37] Andersen Thomas Lund, Andersen Flemming Littrup, Haddock Bryan, et al. Automated quantitative image-derived input function for the estimation of cerebral blood flow using oxygen-15-labelled water on a long-axial field-of-view PET/CT scanner. *Diagnostics.* 2024;14:1590.

[38] Smith Charlotte LC, Zwezerijnen Gerben JC, Hollander Marijke E, et al. Validating image-derived input functions of dynamic 18F-FDG long axial field-of-view PET/CT studies. *Frontiers in Nuclear Medicine.* 2025;5:1556848.

[39] Palard-Novello Xavier, Henrar Rutger B, Oprea-Lager Daniela E, et al. Assessment of fully quantitative and simplified methods for analysis of [68Ga] Ga-FAPI-46 uptake in patients with pancreatobiliary cancer using LAFOV PET/CT. *European Journal of Nuclear Medicine and Molecular Imaging.* 2025;52:1472–1480.

[40] Wu Qi, Gu Fengyun, Wu Yaping, et al. Assessment of Compartmental models and delay estimation schemes for dynamic Total-body PET imaging using uEXPLORER. *Journal of Nuclear Medicine.* 2022;63:3186–3186.

[41] Tomasi Giampaolo, Turkheimer Federico, Aboagye Eric. Importance of quantification for the analysis of PET data in oncology: review of current methods and trends for the future. *Molecular Imaging and Biology.* 2012;14:131–146.

[42] O'Sullivan Finbarr. Imaging radiotracer model parameters in PET: a mixture analysis approach. *IEEE Transactions on Medical Imaging.* 1993;12:399–412.

[43] Moradi Hamed, Vashistha Rajat, O'Brien Kieran, et al. Model selection for dynamic PET compartmental modelling of 18F-FDG uptake using a long axial field-of-view PET scanner with delay and motion correction. *EJNMMI research.* 2025;15:81.

[44] Li Elizabeth J, Spencer Benjamin A, Schmall Jeffrey P, et al. Efficient delay correction for total-body PET kinetic modeling using pulse timing methods. *Journal of Nuclear Medicine.* 2022;63:1266–1273.

[45] Wang Yiran, Spencer Benjamin A, Schmall Jeffrey, et al. High-Temporal-Resolution Lung Kinetic Modeling Using Total-Body Dynamic PET with Time-Delay and Dispersion Corrections. *Journal of Nuclear Medicine.* 2023.

[46] Bhattarai Anjan, Holy Emily Nicole, Li Elizabeth, et al. Comparison of delay correction methods to estimate 18F-florbetaben kinetics in the brain using an image derived input function on total-body EXPLORER PET. *Alzheimer's & Dementia.* 2023;19.

[47] Hinz R., Turkheimer F. E.. Determination of tracer arrival delay with spectral analysis. *IEEE Transactions on Nuclear Science.* 2006;53:212–219.

[48] Turkheimer Federico E, Hinz Rainer, Gunn Roger N, et al. Rank-shaping regularization of exponential spectral analysis for application to functional parametric mapping. *Physics in Medicine & Biology.* 2003;48:3819–3841.

[49] Turkheimer Federico, Sokoloff Louis, Bertoldo Alessandra, et al. Estimation of component and parameter distributions in spectral analysis. *Journal of Cerebral Blood Flow & Metabolism.* 1998;18:1211–1222.

[50] O'Sullivan Finbarr, Gu Fengyun, Wu Qi, et al. A Generalized Linear Modeling Approach to Bootstrapping Multi-frame PET Image Data. *Medical Image Analysis.* 2021:102132.

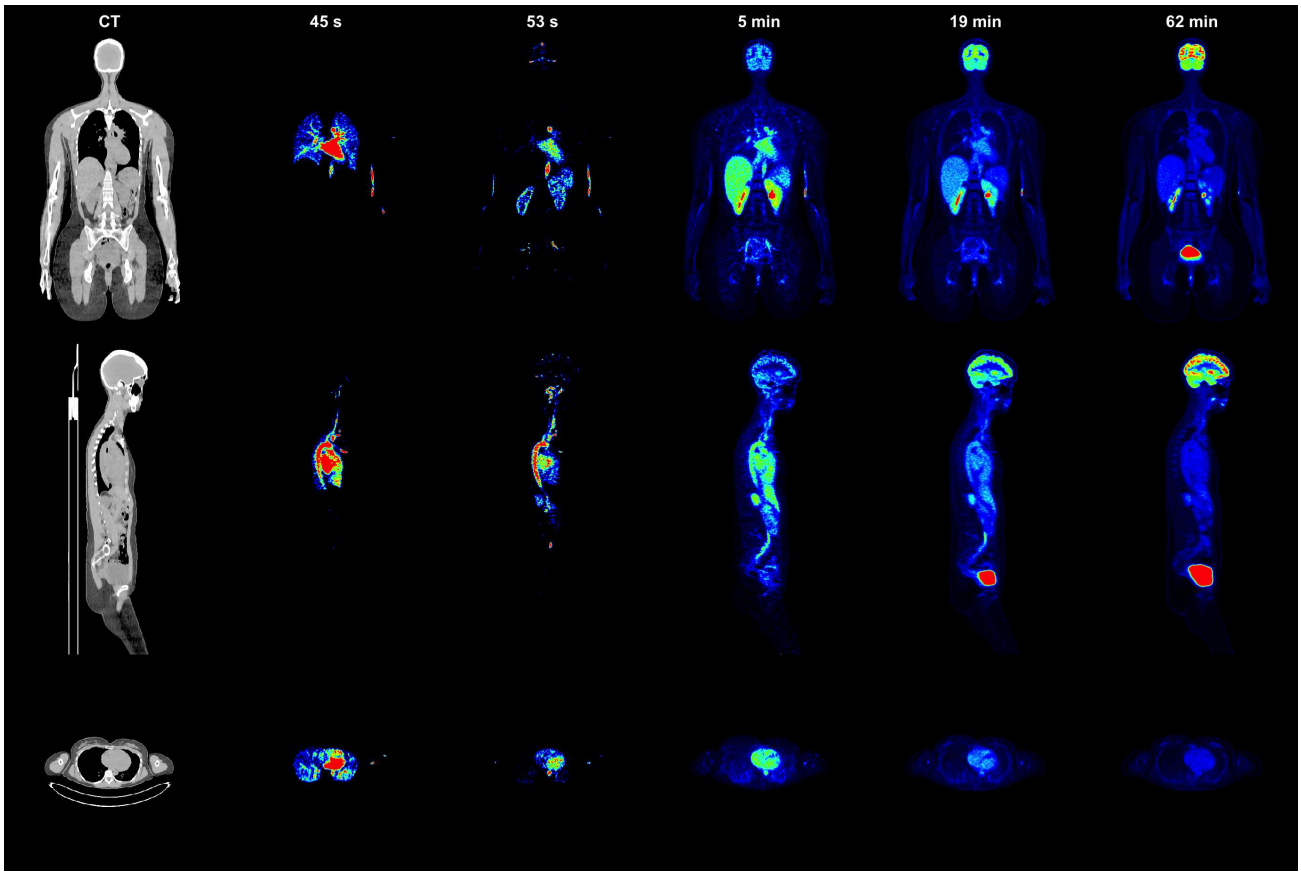

Figure 1: Representative dynamic ^{18}F-FDG images acquired using a LAFOV PET/CT scanner, shown in coronal, sagittal, and axial views at selected time points.

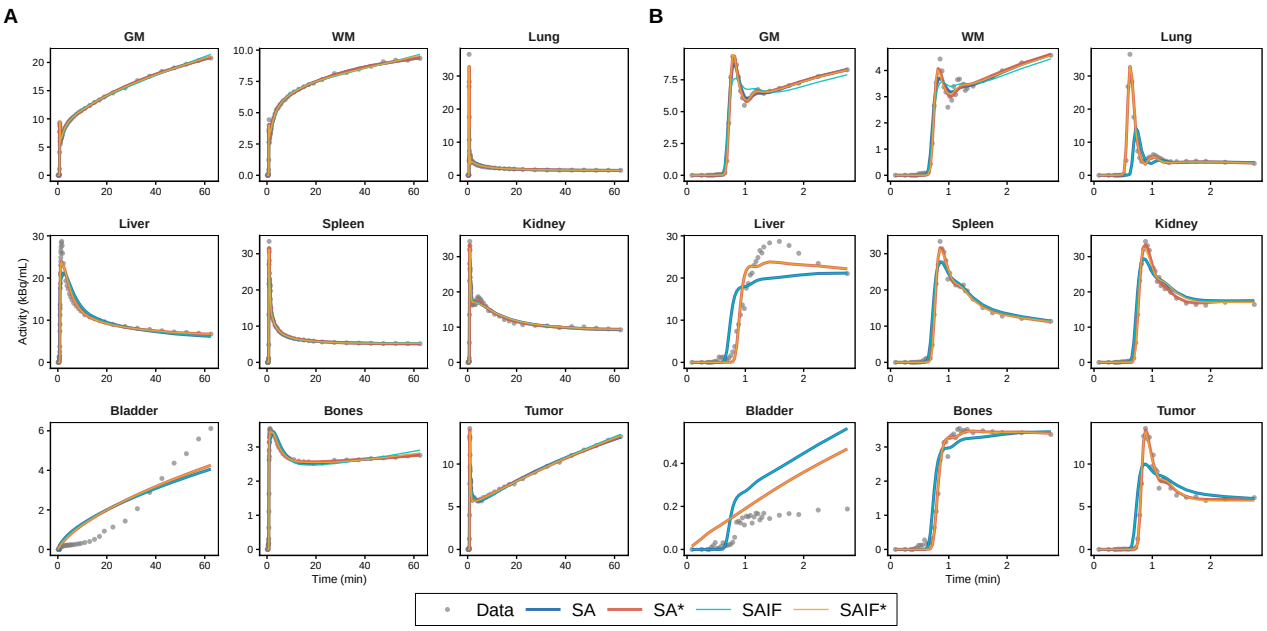

Figure 2: Representative time activity curve fits across nine volumes of interest: gray matter (GM), white matter (WM), lung, liver, spleen, kidney, bladder, bone, and tumor, using four methods: standard spectral analysis (SA), the proposed whole-body adapted spectral analysis (SA*), spectral analysis with iterative filtering (SAIF), and its adapted version (SAIF*). Panel (A) shows the full dynamic acquisition (0–65 min) and panel (B) provides a zoomed view of the early phase (0–3 min).

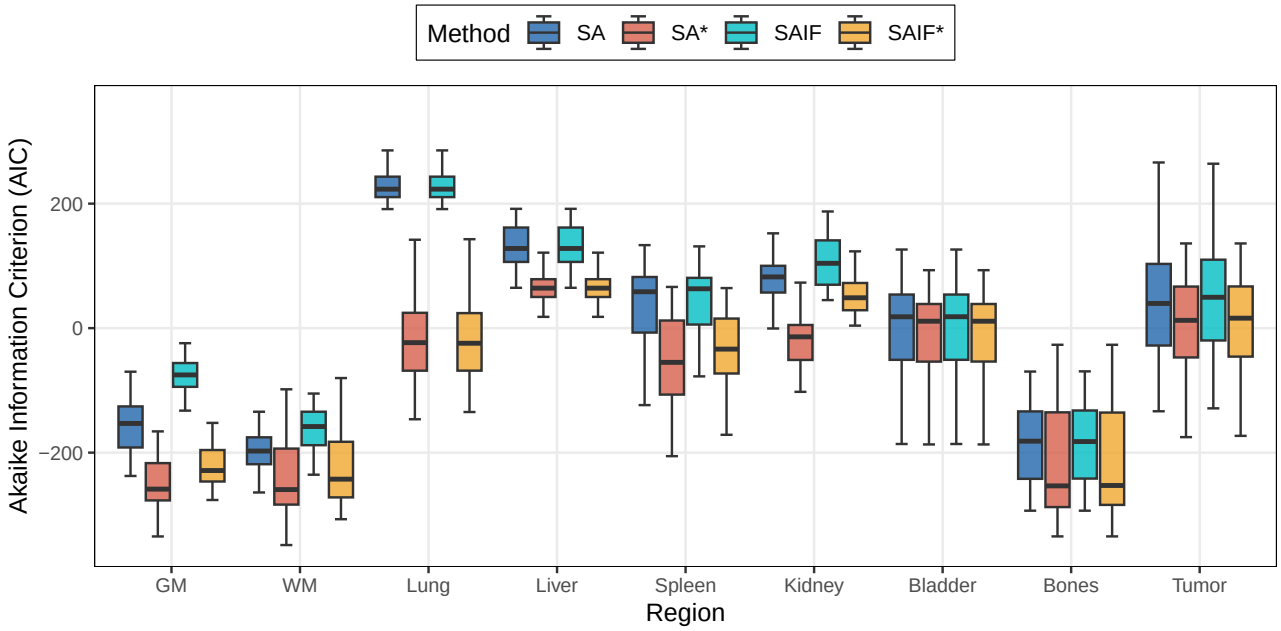

Figure 3: Boxplots of Akaike information criterion (AIC) values across nine VOIs for four methods (SA, SA*, SAIF, SAIF*).

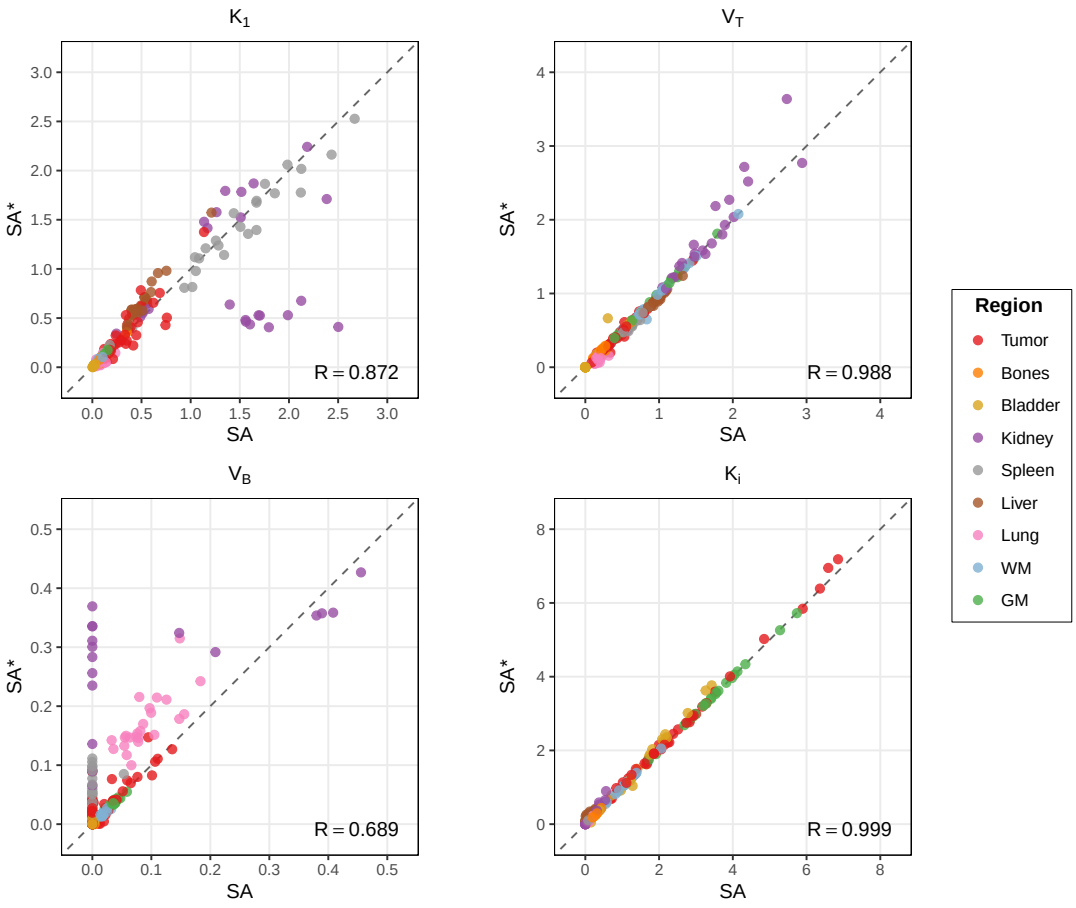

Figure 4: Regional kinetic parameter estimates from SA and SA* across nine volumes of interest in 24 subjects. The four panels compare K_1, V_T, V_B, and K_i and each color denotes one VOI. Pearson correlation coefficients (R) are shown in each panel.

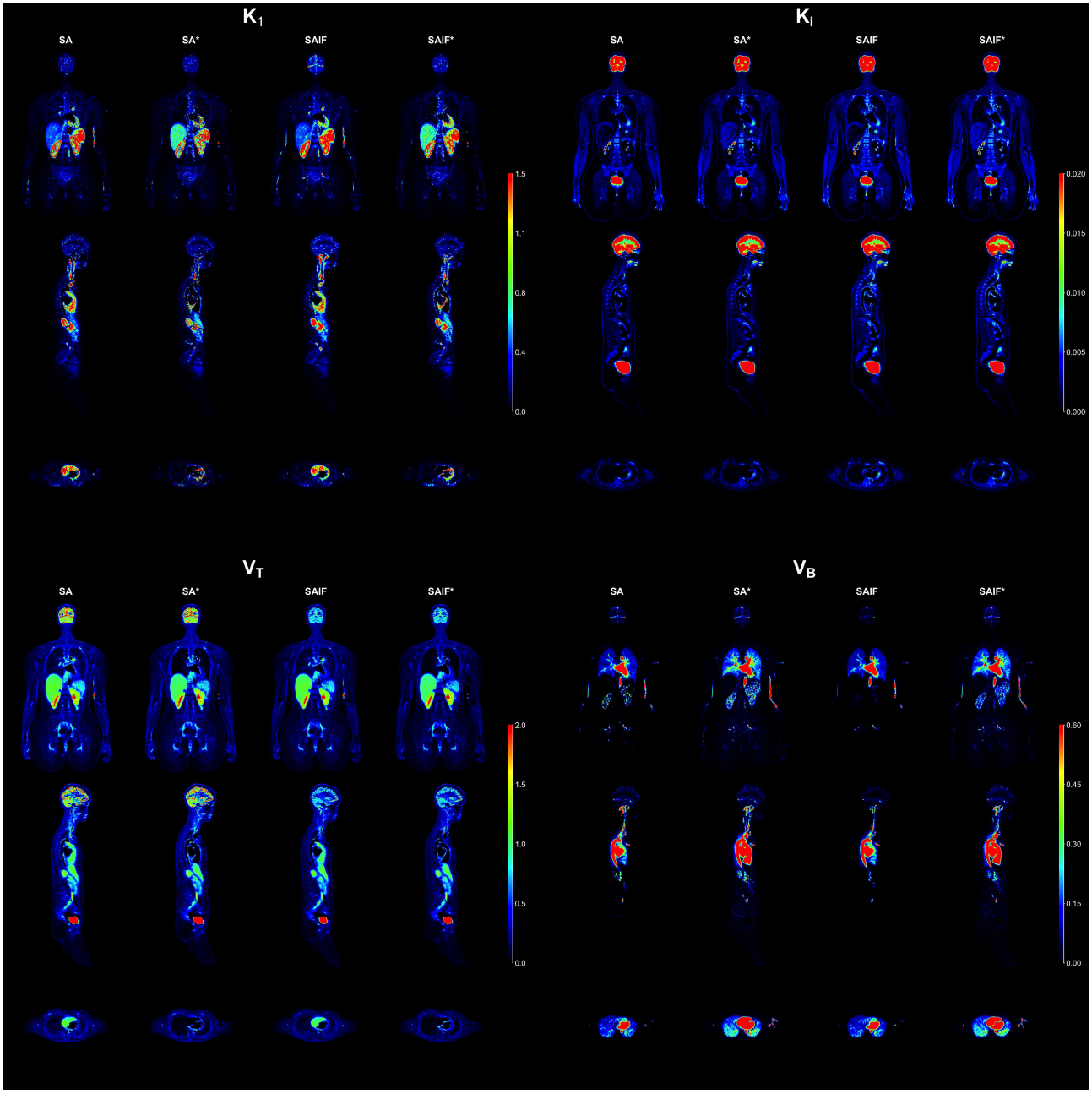

Figure 5: Parametric images of K_1, K_i, V_T, and V_B in sagittal, coronal and axial views, generated by SA, SA*, SAIF and SAIF* for the patient shown in Figure 1.

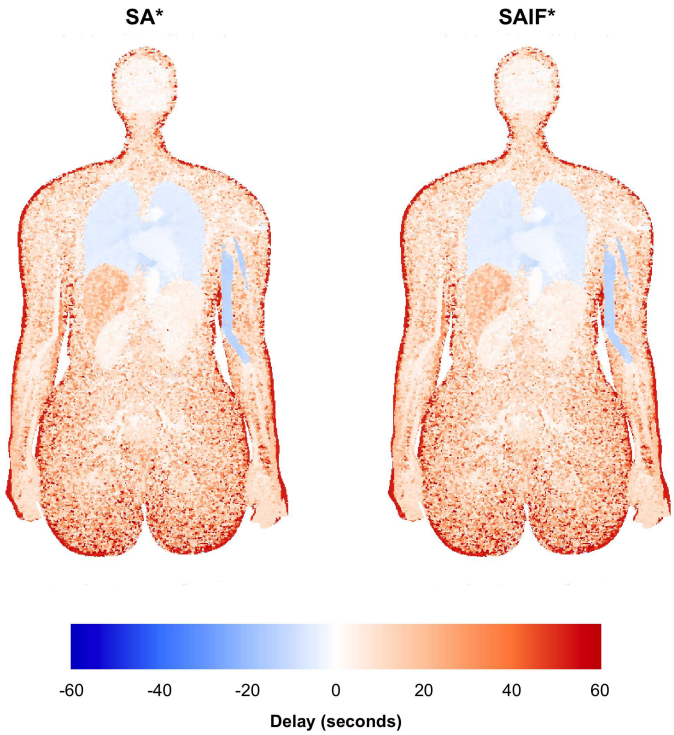

Figure 6: Delay maps (coronal view) estimated using SA* (left) and SAIF* (right) for the same subject. Negative delays (blue) indicate earlier arrival relative to the arterial input reference, whereas positive delays (red) indicate delayed arrival in downstream tissues.

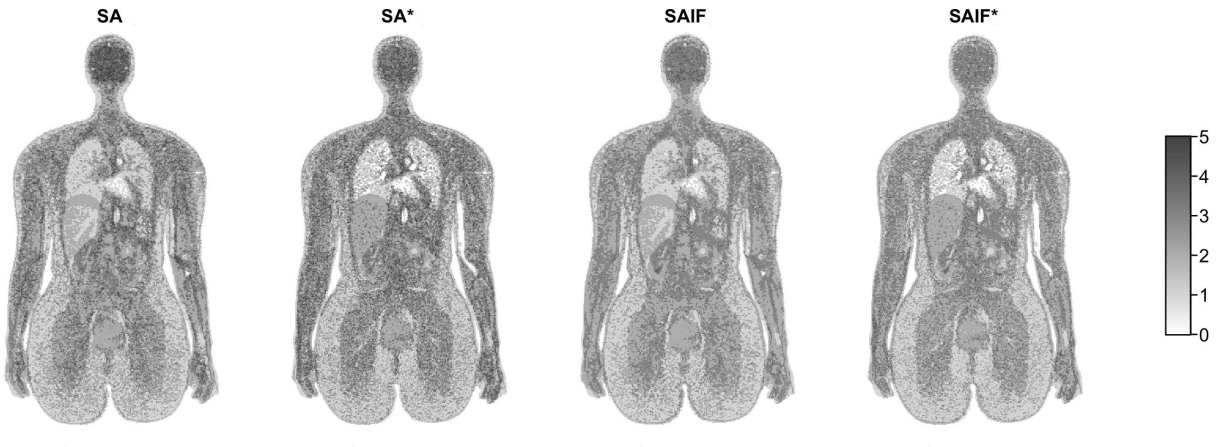

Figure 7: Maps of the optimal number of components (coronal view) estimated using SA, SA*, SAIF, and SAIF* for the same subject.

Table 1: Regional kinetic parameters (mean ± standard deviation) derived from the four spectral analysis methods across nine volumes of interest in 24 subjects. Delay estimates (in seconds) are reported only for the delay-adapted methods (SA* and SAIF*).

Method	VOI	K_1 (mL/min/g)	V_T (mL/g)	V_B (mL/g)	K_i (mL/min/100g)	delay (sec)
	GM	0.15 ± 0.02	0.87 ± 0.40	0.04 ± 0.01	3.36 ± 1.01	
	WM	0.08 ± 0.02	0.91 ± 0.38	0.02 ± 0.01	1.13 ± 0.35	
	Lung	0.09 ± 0.04	0.17 ± 0.04	0.09 ± 0.04	0.08 ± 0.04	
	Liver	0.52 ± 0.18	1.00 ± 0.10	0.00 ± 0.00	0.08 ± 0.09	
SA	Spleen	1.47 ± 0.58	0.64 ± 0.13	0.00 ± 0.01	0.21 ± 0.21	
	Kidney	1.43 ± 0.62	1.62 ± 0.54	0.08 ± 0.16	0.18 ± 0.20	
	Bladder	0.02 ± 0.02	0.06 ± 0.14	0.00 ± 0.00	1.61 ± 0.95	
	Bones	0.11 ± 0.06	0.25 ± 0.10	0.00 ± 0.00	0.28 ± 0.07	
	Tumor	0.33 ± 0.22	0.48 ± 0.26	0.03 ± 0.04	2.50 ± 1.62	
	GM	0.16 ± 0.03	0.88 ± 0.41	0.04 ± 0.01	3.36 ± 1.01	2.33 ± 0.75
	WM	0.09 ± 0.02	0.89 ± 0.39	0.02 ± 0.00	1.14 ± 0.35	2.52 ± 0.95
	Lung	0.06 ± 0.03	0.10 ± 0.03	0.17 ± 0.05	0.08 ± 0.05	−5.81 ± 1.71
	Liver	0.68 ± 0.24	0.94 ± 0.09	0.00 ± 0.00	0.20 ± 0.12	9.15 ± 2.11
SA*	Spleen	1.40 ± 0.55	0.60 ± 0.14	0.06 ± 0.03	0.24 ± 0.21	2.90 ± 1.74
	Kidney	0.96 ± 0.62	1.73 ± 0.69	0.21 ± 0.15	0.24 ± 0.26	2.77 ± 1.58
	Bladder	0.02 ± 0.02	0.08 ± 0.18	0.00 ± 0.01	1.70 ± 1.06	10.83 ± 43.48
	Bones	0.11 ± 0.06	0.24 ± 0.10	0.00 ± 0.00	0.28 ± 0.07	0.88 ± 4.47
	Tumor	0.33 ± 0.25	0.46 ± 0.26	0.04 ± 0.04	2.55 ± 1.66	1.71 ± 4.96
	GM	0.27 ± 0.05	0.53 ± 0.14	0.01 ± 0.01	3.50 ± 0.94	
	WM	0.15 ± 0.03	0.59 ± 0.29	0.00 ± 0.00	1.22 ± 0.40	
	Lung	0.09 ± 0.04	0.16 ± 0.04	0.09 ± 0.04	0.08 ± 0.04	
	Liver	0.52 ± 0.18	1.00 ± 0.10	0.00 ± 0.00	0.08 ± 0.09	
SAIF	Spleen	1.43 ± 0.54	0.60 ± 0.14	0.00 ± 0.00	0.25 ± 0.24	
	Kidney	1.54 ± 0.39	1.52 ± 0.40	0.00 ± 0.01	0.19 ± 0.27	
	Bladder	0.02 ± 0.03	0.04 ± 0.10	0.00 ± 0.00	1.63 ± 0.94	
	Bones	0.11 ± 0.06	0.18 ± 0.05	0.00 ± 0.00	0.33 ± 0.09	
	Tumor	0.37 ± 0.23	0.39 ± 0.18	0.02 ± 0.03	2.56 ± 1.64	
	GM	0.18 ± 0.03	0.62 ± 0.22	0.03 ± 0.01	3.41 ± 1.00	2.88 ± 0.65
	WM	0.10 ± 0.02	0.62 ± 0.28	0.02 ± 0.00	1.18 ± 0.39	3.21 ± 0.92
	Lung	0.06 ± 0.04	0.09 ± 0.03	0.17 ± 0.05	0.09 ± 0.05	−5.77 ± 1.74
	Liver	0.68 ± 0.24	0.94 ± 0.09	0.00 ± 0.00	0.20 ± 0.12	9.15 ± 2.11
SAIF*	Spleen	1.41 ± 0.49	0.58 ± 0.14	0.06 ± 0.04	0.26 ± 0.22	3.48 ± 1.63
	Kidney	1.30 ± 0.28	1.58 ± 0.46	0.12 ± 0.05	0.23 ± 0.32	4.35 ± 1.25
	Bladder	0.02 ± 0.03	0.05 ± 0.11	0.00 ± 0.01	1.71 ± 1.05	10.90 ± 43.46
	Bones	0.11 ± 0.06	0.19 ± 0.05	0.00 ± 0.00	0.32 ± 0.09	1.10 ± 4.55
	Tumor	0.35 ± 0.21	0.38 ± 0.17	0.04 ± 0.04	2.60 ± 1.69	2.11 ± 5.09

Table 2: Regional number of components (mean ± standard deviation) estimated by the four spectral analysis methods across nine volumes of interest in 24 subjects.

VOI	SA	SA*	SAIF	SAIF*
GM	4.2 ± 0.5	4.5 ± 0.7	3.7 ± 0.5	4.0 ± 0.5
WM	4.5 ± 0.7	4.7 ± 0.8	3.7 ± 0.5	3.9 ± 0.4
Lung	1.7 ± 0.6	2.0 ± 0.8	1.6 ± 0.5	1.7 ± 0.6
Liver	1.5 ± 0.5	1.9 ± 0.3	1.5 ± 0.5	1.9 ± 0.3
Spleen	3.0 ± 1.1	4.0 ± 1.1	2.5 ± 0.7	2.9 ± 0.8
Kidney	2.6 ± 0.6	3.0 ± 0.8	2.5 ± 0.5	2.6 ± 0.6
Bladder	1.4 ± 0.7	1.2 ± 0.6	1.3 ± 0.6	1.2 ± 0.6
Bones	3.3 ± 0.8	3.7 ± 1.0	3.0 ± 0.6	3.0 ± 0.6
Tumor	3.4 ± 1.0	3.7 ± 1.1	3.0 ± 0.6	3.1 ± 0.7